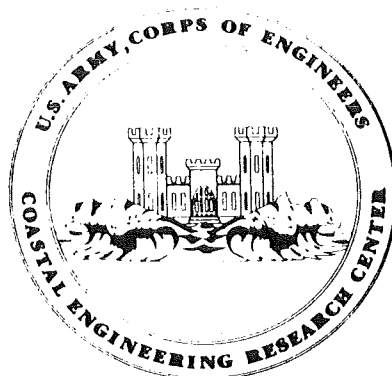


5 MEI 1982

Movable-Bed Laboratory Experiments Comparing Radiation Stress and Energy Flux Factor as Predictors of Longshore Transport Rate

by
Philip Vitale

**MISCELLANEOUS REPORT NO. 81-4
APRIL 1981**



Approved for public release;
distribution unlimited.

**U.S. ARMY, CORPS OF ENGINEERS
COASTAL ENGINEERING
RESEARCH CENTER**

Kingman Building
Fort Belvoir, Va. 22060

MOVABLE-BED LABORATORY EXPERIMENTS COMPARING
RADIATION STRESS AND ENERGY FLUX FACTOR AS PREDICTORS
OF LONGSHORE TRANSPORT RATE

by
Philip Vitale

I. INTRODUCTION

Three-dimensional movable-bed laboratory tests were conducted to compare radiation stress and energy flux factor as predictors of the longshore sediment transport rate. The tests were performed in the U.S. Army Coastal Engineering Research Center's (CERC) Shore Processes Test Basin (SPTB). This report presents derivations of the radiation stress and the energy flux factor, documents the experimental setup and procedure, tabulates most of the data, and performs the data analyses. Many photos were taken during the tests; however, only a few were used in the report. The complete set of test photos is available from CERC's Coastal Engineering Information and Analysis Center (CEIAC).

II. EMPIRICAL RELATIONS

The longshore transport data are related empirically to the two expressions representing wave conditions. One, radiation stress, is based on momentum flux, the other on energy flux. An important concept which is also used in the data analyses is the surf similarity parameter.

1. Momentum Flux.

The dependent variable studied here is the longshore transport rate caused by waves approaching the beach; therefore, the consequential momentum term is the onshore flux of alongshore momentum. The derivation of the term follows Longuet-Higgins (1970) which applies the concept of wave momentum flux to the generation of longshore currents.

The coordinate system used is shown in Figure 1. The y-axis is along the shoreline, the x-axis is normal to the shoreline and positive shoreward, and the z-axis originates at the stillwater level and is positive upward. Using this system, the onshore flux of alongshore momentum is the flux of y-momentum in the x-direction, S_{xy} . This term is one component of what is commonly called the radiation stress tensor.

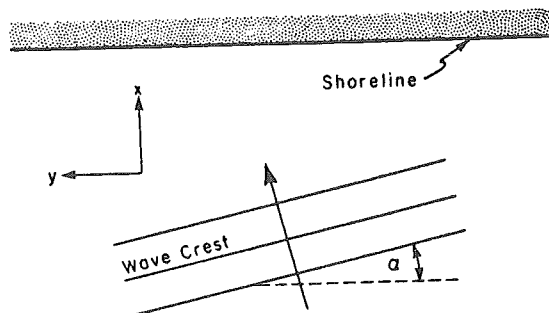


Figure 1. Coordinate system for momentum flux derivation.

According to small-amplitude wave theory, the components of the water particle velocity in the x- and y-directions for a wave traveling at an angle, α , to the shoreline (Fig. 1) are, respectively,

$$u = \frac{H}{2} \frac{gT}{L} \frac{\cosh [k(z+d)]}{\cosh kd} \cos\theta \cos\alpha \quad (1)$$

$$v = \frac{H}{2} \frac{gT}{L} \frac{\cosh [k(z+d)]}{\cosh kd} \cos\theta \sin\alpha \quad (2)$$

where

- H = wave height
- g = acceleration of gravity
- T = wave period
- L = wavelength
- d = water depth
- k = wave number
- θ = wave phase.

The last two terms are defined as

$$k = \frac{2\pi}{L}$$

and

$$\theta = kx - \omega t$$

where t is time, and ω the wave angular frequency

$$\omega = \frac{2\pi}{T}$$

The y-momentum (alongshore momentum) per unit volume is ρv where ρ is the water mass density. The flux of this momentum in the x-direction (onshore) per unit alongshore distance and unit water depth is $\rho v u$. Integrating over the water column and averaging over time produce the mean alongshore momentum flux in the x-direction per unit alongshore distance

$$S_{xy} = \overline{\int_{-d}^{\eta} \rho v u \, dz} \quad (3)$$

where the overbar denotes the mean with respect to time and η the water surface elevation. Substituting equations (1) and (2) into (3) and dropping terms of higher than second order produce

$$S_{xy} = (\overline{EC}_g \cos\alpha) \frac{\sin\alpha}{C} \quad (4)$$

where C is the wave phase velocity, C_g the wave group velocity, and \overline{E} the wave energy density

$$\overline{E} = \frac{\rho g H_{rms}^2}{8} \quad (5)$$

where H_{rms} is the root-mean-square (rms) wave height. The term in parentheses in equation (4) is the flux of wave energy per alongshore distance, F_x , assuming straight and parallel bathymetric contours. When zero wave energy dissipation is assumed,

$$F_x = \overline{EC}_g \cos\alpha = \text{constant} \quad (6)$$

In this report, dissipation is assumed to be zero up to the breaker zone; therefore, F_x is constant from deep water to the breaker zone. Since the ratio of $\sin\alpha$ to C is constant due to Snell's law, equation (4), which represents the alongshore wave momentum entering the surf zone, is constant seaward of the breaker zone.

Equation (4) can be revised for application of monochromatic waves, as in this report. For such wave conditions, the average wave height, \overline{H} , measured during the tests (and discussed later in Section IV) is equal to H_{rms} . By rewriting equation (4),

$$S_{xy} = \left(\frac{\rho g \overline{H}^2}{8} C_g \cos\alpha \right) \frac{\sin\alpha}{C} \quad (7)$$

S_{xy} is now defined for use with laboratory monochromatic wave data. Note that equation (4) is valid for any wave condition; equation (7) is valid only for conditions where \overline{H} equals H_{rms} .

2. Energy Flux.

In literature, the longshore transport rate has been empirically related most frequently to a term found by multiplying both sides of equation (4) by the wave phase velocity, C , to yield

$$P_l = (\overline{EC}_g \cos\alpha) \sin\alpha \quad (8)$$

Unlike S_{xy} , P_l is not constant seaward of the breaker line; therefore, specifying where P_l is being calculated is necessary. This report, following convention, determines P_l at the breaker line,

$$P_{lb} = (\overline{EC}_g \cos\alpha)_b \sin\alpha_b \quad (9)$$

representing the value of P_l at the point closest to where the longshore transport is occurring. The subscript b denotes breaker values. The term

in parentheses in equation (9) has been shown to be constant (see eq. 6) seaward of the breaker line; therefore, subscript b may be replaced by i which represents any point seaward of the breaker line. Making this change, using equation (5), and letting H_{rms} equal \bar{H} for monochromatic waves, equation (9) becomes

$$P_{\ell b} = \left(\frac{\rho g \bar{H}^2}{8} C_g \cos \alpha \right)_i \sin \alpha_b \quad (10)$$

The Shore Protection Manual (SPM) (U.S. Army, Corps of Engineers, Coastal Engineering Research Center, 1977) provides a term similar to $P_{\ell b}$ except that the wave height used is the significant height, H_s . The term, called the longshore energy flux factor, is defined as

$$P_{\ell s} = \left(\frac{\rho g H_s^2}{8} C_g \cos \alpha \sin \alpha \right)_b \quad (11)$$

$P_{\ell s}$ is derived in Galvin and Schweppe (1980). The relationship between H_{rms} and H_s has been shown in Longuet-Higgins (1952) to be

$$H_s^2 = 2H_{rms}^2 \quad (12)$$

assuming a Rayleigh distribution of wave heights as well as a number of other conditions. Therefore,

$$P_{\ell b} = \frac{P_{\ell s}}{2} \quad (13)$$

Since $P_{\ell b}$ and $P_{\ell s}$ are essentially the same terms, this report uses the SPM terminology and refers to $P_{\ell b}$ as the longshore energy flux factor.

3. Longshore Transport Rate.

The longshore transport rate, Q , given in the SPM in units of volume per unit time, is also commonly shown as I_ℓ with units of immersed weight per unit time. The relationship between the two is

$$I_\ell = (\rho_s - \rho) g a' Q \quad (14)$$

where ρ_s is the mass density of sand and a' the ratio of sand volume to total volume of a sand deposit, which takes into account the sand porosity. For discussions of equation (14), see Komar and Inman (1970) and Galvin (1979). Since the laboratory tests described here measured I_ℓ directly, this term is used in most of the data analysis.

4. Empirical Relations.

The expressions derived in the preceding paragraphs are used to set up the following empirical relations

$$I_\ell = K_p P_{\ell b} \quad (15)$$

and

$$I_\ell = K_s S_{xy} \quad (16)$$

where K_p and K_s are coefficients to be determined from the test data in this report.

Equation (15) is based on the concept that the work done in moving the sand alongshore is proportional to the energy which approaches the beach. The units are consistent and K_p is dimensionless.

Equation (16) is based on the concept that the sand transported alongshore depends on the alongshore force exerted by the wave motion on the bed inside the surf zone. By the equation of motion, this force is related to the change of momentum inside the surf zone. The alongshore momentum, S_{xy} , enters the surf zone through the breaker line but cannot exit through the shoreline boundary. Therefore, the change in alongshore momentum is S_{xy} and equation (16) results. K_s has dimensions of length over time.

5. Surf Similarity Parameter.

Kamphuis and Readshaw (1978) showed that K_p and K_s are dependent upon the surf similarity parameter,

$$\xi_b = \frac{\tan \beta}{(H_b/L_o)^{1/2}} \quad (17)$$

in which $\tan \beta$ is the beach slope, H_b the breaker height, and L_o the deepwater ($d/L > 1/2$) wavelength. ξ_b reflects variations in beach shape, breaker type, and rate of energy dissipation. Using the results of laboratory tests, the following relationships were found by Kamphuis and Readshaw

$$K_p = 0.7 \xi_b \quad \text{for} \quad 0.4 < \xi_b < 1.4 \quad (18)$$

$$K_s = 0.08 \xi_b \quad \text{for} \quad 0.4 < \xi_b < 1.25 \quad (19)$$

For values of ξ_b higher than the upper limits, K_p and K_s become independent of ξ_b .

The surf similarity parameter is evaluated in this report to determine its effect on the longshore transport rate.

III. EXPERIMENTAL SETUP

This section discusses the setup in the SPTB (Figs. 2 and 3) and describes the wave generators, wave gages, and cameras and their positions. Also discussed are the sand-moving system, the method for measuring the longshore current velocity, and the size distribution of the sand used in the experiment. The design of the setup was based in large part on Fairchild (1970).

V. DATA

The data collected during the experiments are provided in Appendixes A to D. Appendix A contains the hourly and daily data for each test. Appendix B lists the beach survey data, which are plotted in Appendix C, taken after each test. Appendix D provides 35-millimeter photos of the beach taken during a test with the waves stopped.

1. Hourly and Daily Data in Appendix A.

Table 4 is an example of how the daily and hourly data are tabulated in Appendix A. Column 1 lists the run-time over which the data were collected. Run-time is defined as the cumulative time of wave operation from the beginning of the test. A run-time of 05 10 means that up to that point, waves had been run at the beach for a cumulative total of 5 hours and 10 minutes. This would be the case even if the first wave had been run 2 days before.

Column 2 lists the length of time (in minutes) waves were stopped to take overhead photos of the beach. The letters CFD or TC indicate that the testing was completed for the day or the test was completed. Between any two entries in column 2, the waves were run continuously. For example, from the beginning of the test at run-time 00 00 to run-time 01 00 (see Table 4), the waves were continuously run. At that point the waves were stopped for 5 minutes to take overhead photos of the beach. The waves were then restarted and run continuously until run-time 02 00.

Columns 3 and 4 list the water temperature and the water depth, respectively. These measurements were taken in the morning before the testing started and in the afternoon after the testing stopped.

Column 5 lists the immersed weight of sand moved during testing from the previous entry in the column. A value is always listed with a CFD or TC entry since it was only at the end of the day that the balance of sand not weighed during the time the waves were running could be picked up and weighed. In Table 4, the value of 4,227 immersed pounds of sand is the quantity of sand transported from run-hour 04 00 to 08 00. This column is not a cumulative listing of sand transported.

Columns 6, 7, 8, and 9 list the wave heights measured by gages 1, 2, 3, and 4A or 4B, respectively. Section III discusses the locations of these gages, which are shown in Figure 7. Column 10 lists the breaker angles measured from the Polaroid 4- by 5-inch photos of the breaking waves (see Fig. 16). Column 11 lists the longshore current velocity measured by dye injections, as discussed in Section III. Column 12 lists the breaker type, using the following code: sg, surging; p, plunging; c, collapsing; and sp, spilling. A double entry indicates both types of breakers were evident with the first type predominant.

2. Summary Data Table.

For a comparison of test conditions, Table 3 provides the average values of water temperature, wave height, wave breaker angle, longshore current velocity, and average longshore transport rate in immersed pounds per second for each test. Also included are the wave period and generator angle.

Table 4. Example of hourly and daily data tables in Appendix A.

RUN TIME HR - MIN	MINUTES STOPPED	WATER TEMP CELSIUS	WATER DEPTH CM	PERIOD 1,000 SECONDS	IMMERSED WEIGHT LBS	GENERATOR ANGLE 30 DEGREES				BREAKER ANGLE DEGREES	LONGSHORE CURRENT CM/S	BREAKER TYPE
						GAGE 1	GAGE 2	GAGE 3	GAGE 4A/4B			
0 0		22.7	71.0							15		SG
0 30						6.6	7.0	7.1	7.1			
1 0	5									19		SG
1 30						6.7	6.0	7.3	6.4			
2 0	10									18		SG
2 30						6.1	7.0	7.0	6.1			
3 0	5									16		SG
3 30						6.2	7.0	6.7	6.0			
4 0	CFD	23.1	70.0	4239						19		SG
4 30		22.9	71.0									
5 0						7.2	7.0	5.9	11.9			SG
5 30	10									19		SG
6 0						6.7	6.0	6.1	11.0			
6 30	10									12		SG
7 0						6.6	6.9	6.0	11.9			
7 30	10									13		SG
8 0	CFD	23.1	71.0	4227		7.1	6.0	6.0	11.1			
8 30		23.0	71.0							15		SG
9 0						6.3	7.3	7.0	11.7			
9 30	15									15		SG
10 0						6.2	7.0	7.0	12.2			
10 30	CFD	23.8	70.0	1601						20		SG
11 0		23.7	71.0									
11 30	10					6.5	6.0	6.2	10.8			
12 0										14		SG
12 30	10					7.2	6.5	6.8	6.9			
13 0										16	10	SG
13 30	10					7.1	6.4	6.9	6.4			
14 0										16		SG
14 30	CFD	23.5	71.0	3500		7.0	6.0	6.0	6.1			
15 0		23.5	71.0							18		SG
15 30	10									16		SG
16 0						6.8	6.8	6.4	6.0			
16 30	10									19		SG
17 0						6.5	6.7	5.8	6.0			
17 30	10									18		SG
18 0	CFD	22.8	71.0	3635		6.2	6.7	6.8	10.0			
18 30		22.8	71.0							19		SG
19 0						6.0	7.0	6.1	6.4			
19 30	20									18		SG
20 0						6.5	7.1	6.2	6.5			
20 30	10									14		SG
21 0						5.9	7.8	7.3	7.5			
21 30	10									12		SG
22 0	CFD	23.1	71.0	3769		5.8	6.2	7.2	6.0			
22 30										13		SG
23 0						5.7	7.6	6.5	6.8			
23 30	5									11		SG
24 0	TC	23.1	71.0	1000		6.2	7.9	7.7	7.3			

1CFD = testing completed for day; TC = testing completed.

3. Survey Data.

After each test, the SPTB was drained and the beach was surveyed. The distance and elevation pairs are listed in Appendix B and plotted in Appendix C. The elevation datum is the stillwater level (SWL), which corresponded to a 0.710-meter water depth.

4. Overhead Photos.

Every hour during testing, the waves were stopped to take an overhead 35-millimeter photo of the beach (see Fig. 15). The photos show the waterline, the longshore bar, and the swash zone. They are useful for a qualitative description of how the beach responded to the waves. Appendix D contains a series of photos for run-times 01 00, 08 00, 16 00, and 24 00.

VI. DATA ANALYSIS

This section includes the data analysis to determine the relations between I_L and S_{xy} and I_L and P_{lb} . The empirical coefficients found from these relations are then, in turn, related to the surf similarity parameter, ξ , which is adapted to the data collected. Also included is an explanation of the calculations of S_{xy} , P_{lb} , ξ , and I_L , along with plots of the various relationships. The wave height used in the calculations is that measured at the toe of the beach (average of gages 1 and 2 wave heights). The breaker wave height, which would have been a better value, was not used for the following reasons. The wave height at the toe of the beach was measured for all 15 tests; the breaker height was not. Also, only one gage was used to measure breaker height, while two were used at the beach toe. The significant difference in height between waves measured at the two beach toe gages (see App. A) indicates that some wave height variability existed along the wave crest. Therefore, the average of the measurements at the two beach toe gages is probably a more reliable estimate of the entire wave passing the toe than the one gage measurement at the breaker is of the entire breaker wave. A comparison of the data in this report with past studies is shown in a Q versus P_{lb} graph.

1. Calculation of S_{xy} .

Equation (7)

$$S_{xy} = \left(\frac{\rho g \bar{H}^2}{8} C_g \cos \alpha \right) \frac{\sin \alpha}{C}$$

was used to calculate S_{xy} . Rearranging the equation,

$$S_{xy} = \frac{\rho g}{16} \bar{H}^2 n \sin 2\alpha \quad (21)$$

where n is the ratio C_g/C and a function of the water depth and wave period or length. S_{xy} was calculated at the toe of the beach by using the average of the wave heights measured at that location (see Fig. 7), and by using the generator angle for α . This was calculated for each set of wave data. Thus, for the standard 24-hour test, 24 values of S_{xy} were calculated (see App. E). The average of S_{xy} for each test is listed in Table 5.

Table 5. Test cycle calculations.

Test	Total run time (hr)	S_{xy} (N/m)	P_{lb} (J/m/s)	I_{ξ} (N/s)	K_s (m/s)	K_p	ξ
1	25	1.179	2.201	0.6116	0.5190	0.2779	0.6604
2	30	1.137	2.043	0.6889	0.6058	0.3373	0.6686
3	24	2.280	3.232	0.8396	0.3682	0.2598	0.3374
4	24	2.158	3.615	0.6188	0.2868	0.1712	0.4508
5	24	0.987	0.789	0.7544	0.7640	0.9557	0.8997
6	24	1.977	2.144	0.9966	0.5042	0.4648	0.6815
7	24	3.161	4.158	0.7281	0.2303	0.1751	0.4787
8	24	3.018	3.918	0.3446	0.1142	0.0880	0.4835
9	24	2.808	4.286	0.5227	0.1862	0.1220	0.3761
10	24	8.250	14.761	1.0605	0.1285	0.0718	0.3764
12	24	2.942	4.839	1.6328	0.5550	0.3374	0.6644
13	24	2.241	2.948	1.1941	0.5328	0.4051	0.9190
14	24	11.578	28.802	3.2938	0.2845	0.1144	0.6112
15	24	9.253	13.536	2.5502	0.2756	0.1884	0.3934

2. Calculation of P_{lb} .

Equation (10)

$$P_{lb} = \left(\frac{\rho g \bar{H}^2}{8} C_g \cos \alpha \right)_i \sin \alpha_b$$

was used to calculate P_{lb} . The term in the parentheses, like S_{xy} , was calculated at the toe of the beach. However, the sine term used the breaker angle as measured from the photos of the breaking waves. The breaker angle used in the calculation was the average of the breaker angles collected 30 minutes before and after the wave data were collected (see Fig. 14). P_{lb} was calculated for each set of wave data, 24 values of P_{lb} were calculated for the standard 24-hour test (see App. E). The average of P_{lb} for each test is listed in Table 5.

3. Calculation of ξ .

The surf similarity parameter of Kamphuis and Readshaw (1978) was presented in equation (17) as

$$\xi_b = \frac{\tan \beta}{(H_b/L_o)^{1/2}}$$

For the data in this report, a different surf similarity parameter is needed since \bar{H} will be substituted for H_b , as discussed at the beginning of this section. Therefore, the surf similarity parameter in the following analysis is

$$\xi = \frac{\tan \beta}{(\bar{H}/L_o)^{1/2}} \quad (22)$$

The same beach slope was used for all 15 tests and was determined as shown in Figure 21. A value of ξ was calculated for each test using the average \bar{H} for the entire test. These values are listed in Table 5.

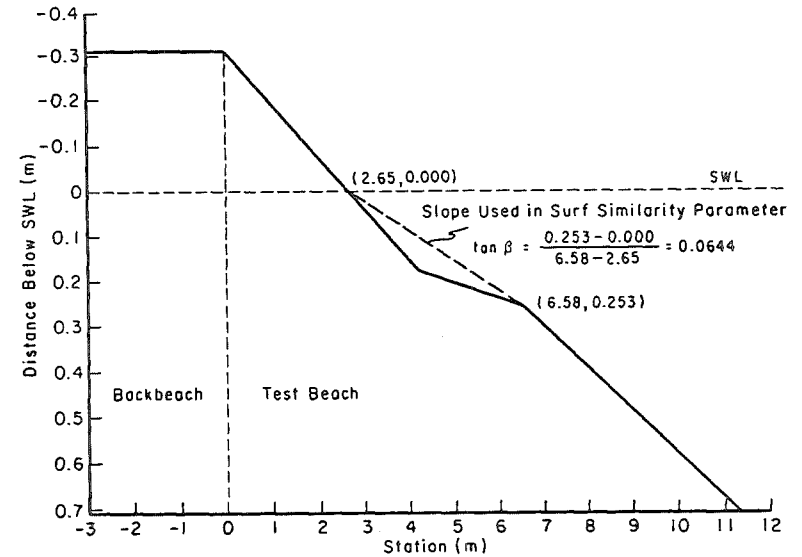


Figure 21. Determination of beach slope used to calculate the surf similarity parameter.

4. Special Tests.

Three tests were performed under special circumstances. Test 2 was a repeat of test 1; test 8 was a repeat of test 7, except the sand feeder was moved shoreward; and test 11 was done with a generator angle of zero.

Tests 1 and 2 were both run with a period of 2.35 seconds, a generator angle of 10° , and a generator eccentricity of 5.97 centimeters. Test 1 ran for 25 hours, test 2 for 50 hours. A twofold comparison of the two tests was originally planned. The first 25 hours of test 2 data was to be compared to the test 1 data, and then, both sets of data were to be compared to the last 25 hours of test 2. Unfortunately, due to an experimental error, only the first 30 hours of the test 2 longshore transport data was collected accurately. Therefore, the only comparison made was test 1 to the first 30 hours of test 2. Reference to test 2 in the remainder of the report refers to the first 30 hours only. Appendix A contains all 50 hours of test 2 data.

Table 6 compares the results of the two tests. The differences listed give an indication of the repeatability of the data collection. The longshore transport rate changed by 12.6 percent, which is a significant variation. This is an inherent problem of longshore transport tests, indicating that some important unknown factors are at work.

Table 6. Comparison of tests 1 and 2.

Test	Total run-time (hr)	Avg H (cm)	Avg α_b (degrees)	I_ℓ (N/s)	S_{xy} (N/m)	$P_{\ell b}$ (J/m/s)
1	25	8.17	8	0.612	1.18	2.20
2	30	8.03	7	0.689	1.14	2.04
Pct difference ¹		-1.7	-12.5	+12.6	-3.4	-7.3

$$^1\text{Pct difference} = \frac{(\text{Test 1} - \text{Test 2})}{\text{Test 1}} \cdot 100.$$

Tests 7 and 8 were both run with a period of 1.90 seconds, a generator angle of 20°, and a generator eccentricity of 5.97 centimeters. The only difference was that the sand feeder, which was located at the SWL for all other tests, was moved shoreward 1.4 meters for test 8. The feeder was moved because the shoreline at the end of test 7 significantly angled shoreward toward the downdrift side of the beach. This can be seen in the test 7 photos in Appendix D. The feeder was moved shoreward to see if a straight shoreline resulted. It did, as the photos in Appendix D for test 8 show. Another major effect was the change in I_ℓ from 0.728 newton per second for test 7 to 0.345 newton per second for test 8, a decrease of 53 percent. Test 8 is excluded from the remaining data analyses.

Test 11 was run with a period of 2.35 seconds, a generator angle of 0°, and a generator eccentricity of 5.97 centimeters. The test was meant as a control to determine the amount of sand moved by the diffusion caused by breaking waves. This value of I_ℓ for test 11 was 0.089 newton per second. A comparable quantity of sand, 0.059 newton per second, also moved updrift. Test 11 is also excluded from the remaining data analyses.

5. Daily Cycle Graphs.

As discussed previously, longshore transport could be measured only on a daily cycle or test cycle basis. For the typical 24-hour test, six values of longshore transport rate were calculated. Each rate covered a period of 4 run-hours. During this time period, four values of S_{xy} and $P_{\ell b}$ were calculated, averaged, and related to the corresponding value of I_ℓ . These values are listed in Appendix F and plotted in Figures 22 and 23. Table 7 lists the important statistical parameters.

Table 7. Daily cycle statistics.

Relation	Figure No.	r^2	Least squares lines		
			Standard slope	Y-intercept	Through origin slope
I_ℓ versus S_{xy}	22	0.74	0.21	0.38	0.28
I_ℓ versus $P_{\ell b}$	23	0.73	0.09	0.58	0.13

The square of the correlation coefficients, r^2 , represents the fraction of the variation of I_ℓ about its mean which is explained by the abscissa term. r^2 for S_{xy} and $P_{\ell b}$ are 0.74 and 0.73, respectively. These numbers show that I_ℓ correlates well with both terms to approximately equal degrees. The least squares lines listed in Table 7 are in Figures 22 and 23, which also include the least squares lines calculated with the limitation that the lines pass through the origin. The slopes of these lines are 0.28 for the I_ℓ versus S_{xy} graph and 0.13 for the I_ℓ versus $P_{\ell b}$ graph.

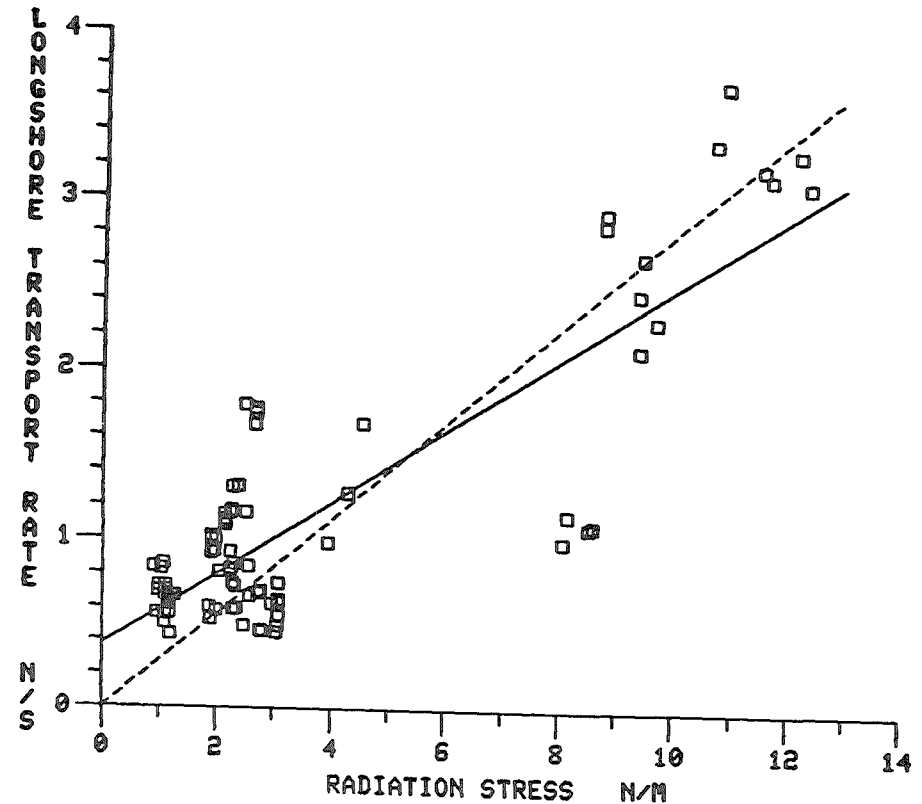


Figure 22. Relation between longshore transport rate, I_ℓ , and radiation stress, S_{xy} , using daily cycle data (tests 8 and 11 excluded).

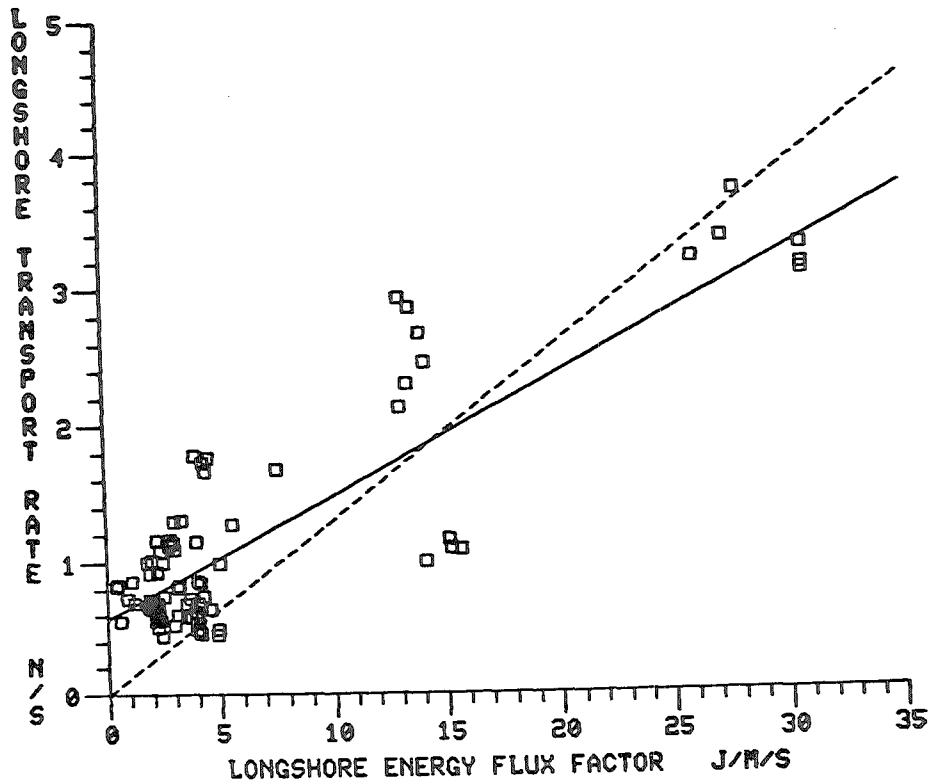


Figure 23. Relation between longshore transport rate, I_l , and longshore energy flux factor, P_{lb} , using daily cycle data (tests 8 and 11 excluded).

6. Test Cycle Graphs.

The average longshore transport rate for each test was calculated and compared with the test average of S_{xy} and P_{lb} . These values are listed in Table 5 and plotted in Figures 24 and 25. Statistical values are in Table 8. r^2 for I_l versus S_{xy} and I_l versus P_{lb} are 0.72 and 0.74, respectively. As with the daily cycle calculations, I_l is shown to correlate well with both terms to approximately equal degrees. Figures 24 and 25 include both the standard least squares line and the least squares line forced through the origin. The slopes of the latter lines are 0.26 for the I_l versus S_{xy} graph and 0.13 for the I_l versus P_{lb} graph.

Table 8. Text cycle statistics.

Relation	Figure No.	r^2	Least squares lines		
			Standard slope	Y-intercept	Through origin slope
I_l versus S_{xy}	24	0.72	0.21	0.40	0.26
I_l versus P_{lb}	25	0.74	0.09	0.58	0.13
K_s versus ξ	26	0.70	0.82	-0.07	
K_p versus ξ	27	0.56	0.89	-0.22	

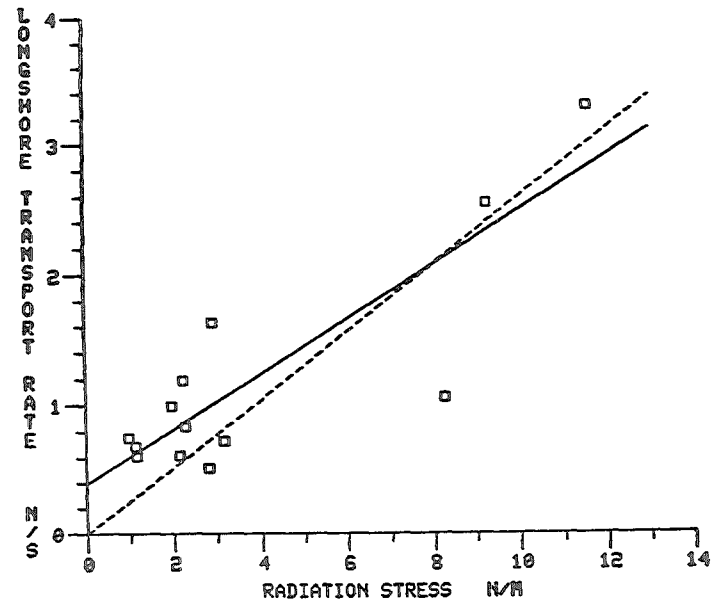


Figure 24. Relation between longshore transport rate, I_l , and radiation stress, S_{xy} , using test cycle data (tests 8 and 11 excluded).

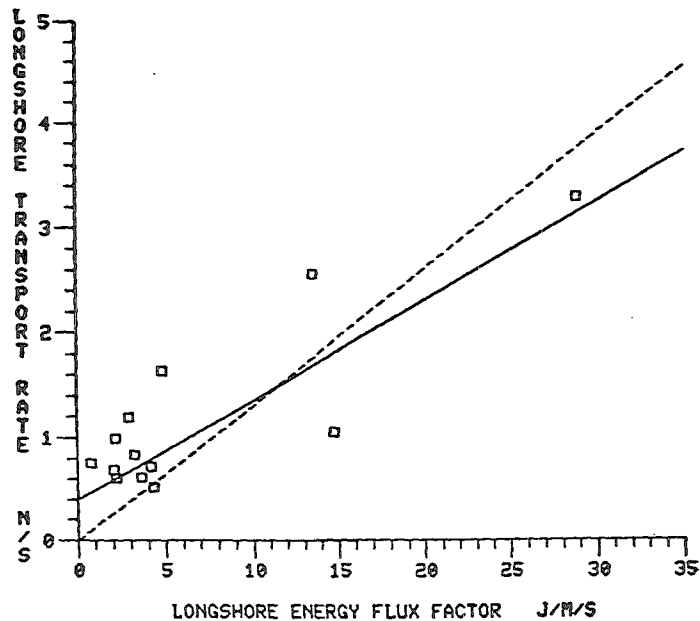


Figure 25. Relation between longshore transport rate, I_L , and longshore energy flux factor, P_{lb} , using test cycle data (tests 8 and 11 excluded).

7. Surf Similarity Relation.

Figures 26 and 27 were drawn to test the dependence of K_S and K_P on ξ . Test numbers are indicated in the figures. Table 8 lists the statistics. The K terms were calculated using equations (15) and (16). These graphs show that K is far from being constant, as is commonly assumed, and that it is strongly related to ξ .

8. Comparison to Past Data.

The units of I_L and P_{lb} were converted to those used in the SPM and plotted in Figure 28, which is taken from Figure 4-36 of the SPM. The SPM figure was modified by shifting the x-axis to convert from P_{ls} to P_{lb} . Equation (13) shows the relation between P_{lb} and P_{ls} . Test numbers for the data points of this report are noted in Figure 28.

Two major observations are immediately apparent. The first is that the laboratory data in this report, as in laboratory data from past reports, have considerable scatter. Since the surf similarity parameter, ξ , in this report varies by a significant amount for the different tests, as shown in Figures 26 and 27, some scatter is expected. The surf similarity parameter, of course, does not explain all of the scatter in the laboratory data. There are still some laboratory and scale effects which are not yet understood.

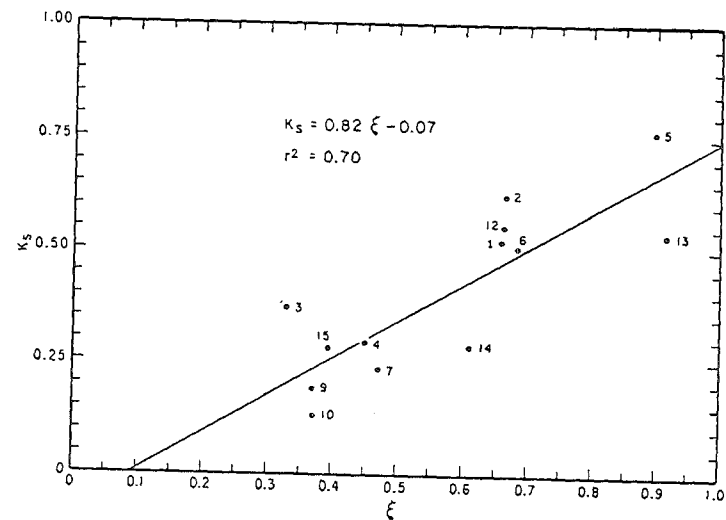


Figure 26. Relation between K_S and the surf similarity parameter, ξ , using test cycle data (tests 8 and 11 excluded).
43

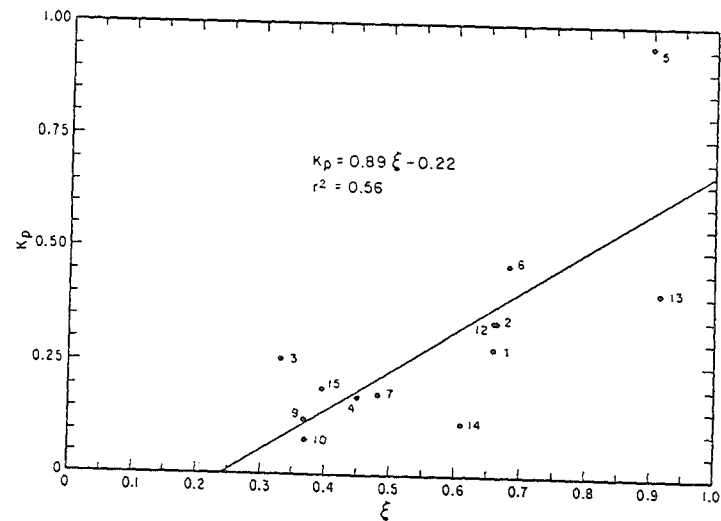


Figure 27. Relation between K_P and the surf similarity parameter, ξ , using test cycle data (tests 8 and 11 excluded).

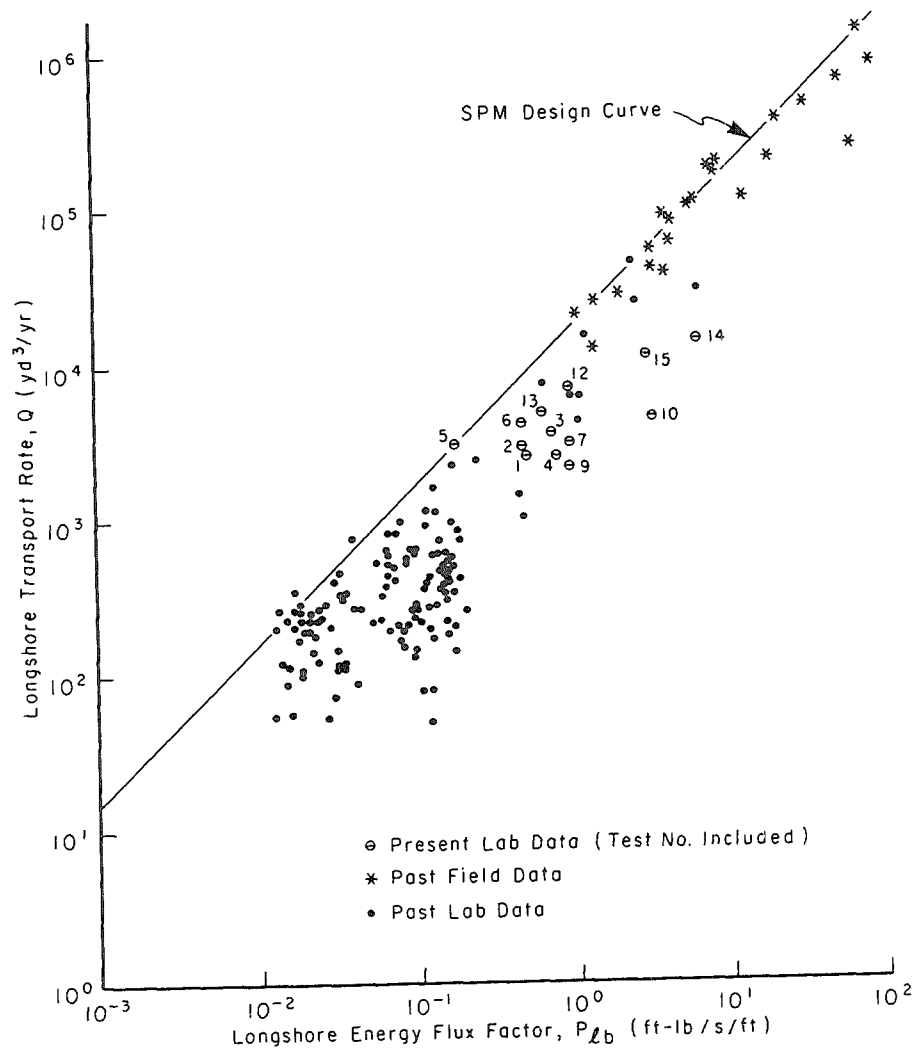


Figure 28. Comparison of data in this report to past reports, using SPM Figure 4-36 (tests 8 and 11 excluded).

The second observation is that most of the data fall beneath the SPM curve connoting low values of K_p . Since the SPM curve is based on field data, mostly from Komar and Inman (1970), a possible explanation is that the field data were collected under conditions of higher values of ξ than those for the laboratory data. Kamphuis and Readshaw (1978) suggest that Komar and Inman's data were indeed collected under conditions of high ξ_b . It seems reasonable to assume that the ξ values were also high.

VII. SUMMARY AND CONCLUSIONS

An analysis of the radiation stress, S_{xy} , and the energy flux factor, P_{lb} , shows that both predict longshore transport rate, I_l , to comparable degrees. Approximately 70 percent of the variance of I_l about its mean is explained by each term. There appears to be no major advantage in choosing one over the other to predict the longshore transport rate. However, S_{xy} has the advantage of being constant seaward of the breaker zone while P_{lb} is not. This makes the calculation of S_{xy} more convenient than P_{lb} , which must be determined at the breaker line. On the other hand, P_{lb} has the advantage of having the same units as I_l , which means that K_p is dimensionless.

The empirical coefficients, K_s and K_p , are far from constant although K_p is commonly assumed to be so in practice. Part of the variation of the coefficients can be related to the variation of the surf similarity parameter, ξ , as shown in Figures 26 and 27. These figures show that K_s and K_p will increase with ξ . The considerable scatter evident in Figure 28 can be partly explained by the relation between the empirical coefficients and ξ . The data in this report and past laboratory and field data are compared in Figure 28. The laboratory data generally predict lower values of I_l for a given P_{lb} compared to the field data. Part of this trend can be explained by the differences in the surf similarity parameters, assuming the field data were collected under conditions of high ξ . Also, laboratory and scale effects probably contribute to the lower laboratory transport rates. The relative importance of these factors is suggested as a subject of future research.

LITERATURE CITED

- CHESNUTT, C.B., "Analysis of Results from 10 Movable-Bed Experiments," Vol. VIII, MR 77-7, *Laboratory Effects in Beach Studies*, U.S. Army, Corps of Engineers, Coastal Engineering Research Center, Fort Belvoir, Va., June 1978.
- FAIRCHILD, J.C., "Laboratory Tests of Longshore Transport," *Proceedings of the 12th Conference on Coastal Engineering*, American Society of Civil Engineers, Vol. II, 1970, pp. 867-889.
- GALVIN, C.J., "Relation Between Immersed Weight and Volume Rates of Longshore Transport," TP 79-1, U.S. Army, Corps of Engineers, Coastal Engineering Research Center, Fort Belvoir, Va., May 1979.
- GALVIN, C.J. Jr., and EAGLESON, P.S., "Experimental Study of Longshore Currents on a Plane Beach," TM-10, U.S. Army, Corps of Engineers, Coastal Engineering Research Center, Washington, D.C., Jan. 1965.
- GALVIN, C. and SCHWEPPE, C.R., "The SPM Energy Flux Method for Predicting Longshore Transport Rate," TP 80-4, U.S. Army, Corps of Engineers, Coastal Engineering Research Center, Fort Belvoir, Va., June 1980.
- KAMPHUIS, J.W., and READSHAW, J.S., "A Model Study of Alongshore Sediment Transport Rate," *Proceedings of the 16th Conference on Coastal Engineering*, American Society of Civil Engineers, Vol. II, 1978, pp. 1656-1674.
- KOMAR, P.D., and INMAN, D.L., "Longshore Sand Transport on Beaches," *Journal of Geophysical Research*, Vol. 75, No. 30, Oct. 1970, pp. 5914-5927.
- LONGUET-HIGGINS, M.S., "On the Statistical Distribution of the Height of Sea Waves, 1," *Journal of Marine Research*, Vol. 11, 1952, pp. 245-266.
- LONGUET-HIGGINS, M.S., "Longshore Currents Generated by Obliquely Incident Sea Waves," *Journal of Geophysical Research*, Vol. 75, No. 33, Nov. 1970, pp. 6778-6801.
- SAVAGE, R.P., "A Sand Feeder for Use in Laboratory Littoral Transport Studies," *The Annual Bulletin of the Beach Erosion Board*, Vol. 15, U.S. Army, Corps of Engineers, Washington, D.C., July 1961.
- STAFFORD, R.P., and CHESNUTT, C.B., "Procedures Used in 10 Movable-Bed Experiments," Vol. I, MR 77-7, *Laboratory Effects in Beach Studies*, U.S. Army, Corps of Engineers, Coastal Engineering Research Center, Fort Belvoir, Va., June 1977.
- U.S. ARMY, CORPS OF ENGINEERS, COASTAL ENGINEERING RESEARCH CENTER, *Shore Protection Manual*, 3d ed., Vols. I, II, and III, Stock No. 008-022-00113-1, U.S. Government Printing Office, Washington, D.C., 1977, 1,262 pp.